Non-parametric system norm estimation of multivariable systems

Tacx, Paul; Oomen, Tom

DOI
10.1016/j.conengprac.2025.106421

Publication date
2025

Document Version
Final published version

Published in
Control Engineering Practice

Control Engineering Practice 164 (2025) 106421

Contents lists available at ScienceDirect

Control Engineering Practice

journal homepage: www.elsevier.com/locate/conengprac

Non-parametric system norm estimation of multivariable systems☆

Paul Tacx [a,*], Tom Oomen [b,c]

[a] ASML, Development and Engineering, Mechatronics and Measurement Systems, Veldhoven, The Netherlands
[b] Department of Mechanical Engineering, Eindhoven University of Technology, Eindhoven, The Netherlands
[c] Faculty of Mechanical, Maritime, and Materials Engineering, Delft University of Technology, Delft, The Netherlands

ARTICLE INFO

Keywords:
Identification for control
Multivariable control systems
Robust control
Control applications
Local parametric modeling
Motion control

ABSTRACT

Data-driven estimation of system norms is essential for analyzing, verifying, and designing control systems. Existing data-based methods often do not capture the inter-grid and transient behavior of the system, leading to inaccurate and unreliable system norm estimations. This paper presents a unified approach for accurate and reliable estimation of the $\mathcal{H}_2$ and $\mathcal{H}_\infty$ norm with a limited amount of data. The key step is to exploit local parametric models that explicitly incorporate the inter-grid and transient dynamics. The system norm is estimated through the computation of local system norms of the local parametric models within their the local frequency interval. Simulation and experimental results illustrate the effectiveness of the proposed method.

1. Introduction

Accurate and precise estimation of system norms is essential in many control and system analysis applications (Gawronski, 2004; Skogestad & Postlethwaite, 2005; Zhou & Doyle, 1998). The $\mathcal{H}_\infty$ and $\mathcal{H}_2$ norms, in particular, are crucial in various applications. For instance, the accurate and precise estimation of the $\mathcal{H}_\infty$ norm is key for robust control design to ensure robustness and performance. Underestimation can lead to instability, while overestimation results in overly conservative robust control design (Vinnicombe, 2001). Conversely, the accurate and precise $\mathcal{H}_2$-norm estimation is critical for model reduction (Antoulas, 2005; Gawronski, 2004). In addition, specific applications may require focusing on a particular frequency range. This can be attributed to limitations in the model of the system and operating conditions, or specific design objectives and considerations. Therefore, the aim of this paper is to develop a method for accurate and robust estimation of the global and finite-frequency $\mathcal{H}_2$ and $\mathcal{H}_\infty$ norm.

Traditionally, data-driven approaches have been used to estimate system norms in practice. Based on an experimentally determined frequency response function estimate the $\mathcal{H}_\infty$ and $\mathcal{H}_2$ norms are estimated in Anderson, Emami-Naeni, and Vincent (1991) and Van de Wal, van Baars, Sperling, and Bosgra (2002). However, only frequencies in the Discrete Fourier Transform (DFT) grid are considered due to the finite measurement time. As a result, these frequency response-based approaches do not include the inter-grid behavior, which leads to unreliable norm estimates, especially for lightly-damped system behavior. Additionally, the transient system behavior is not included in these frequency response function-based methods, which leads to an additional bias in the system norm estimate. The inter-grid behavior is estimated in Vries and Van Hof (1994) based on a deterministic worst-case approach. However, these approaches often result in significant overestimation of the $\mathcal{H}_\infty$ norm (Friedman & Khargonekar, 1995; Vinnicombe, 2001).

Data-driven iterative methods for $\mathcal{H}_\infty$ norm estimation, as proposed in Müller and Rojas (2019), Oomen, van der Maas, Rojas, and Hjalmarsson (2014), Oomen and Rojas (2023) and Wahlberg, Syberg, and Hjalmarsson (2010), mitigate this problem by taking the inter-grid behavior into account through dedicated experiments. However, these methods rely on a series of experiments that inflate significantly for multivariable systems. Alternatively, Gaussian process-based methods can be employed to estimate system norms, see, e.g., Persson, Koch, and Allgöwer (2020) for $\mathcal{H}_2$ norm estimation and Devonport, Seiler, and Arcak (2023) for $\mathcal{H}_\infty$-norm estimation. However, such probabilistic methods are not considered in this paper, and a deterministic approach is pursued.

Alternatively, system norms can be determined with techniques based on the availability of parametric system descriptions. In Antoulas (2005, Section 5) and Gawronski (2004, Section 6), parametric methods are considered for calculating the $\mathcal{H}_2$ norm. Similarly, $\mathcal{H}_\infty$-norm estimation methods based on parametric system descriptions has been proposed in Boyd, Balakrishnan, and Kabamba (1989), Bruinsma

☆ This work is part of the research programme VIDI with project number 15698, which is (partly) financed by the Netherlands Organisation for Scientific Research (NWO).

* Corresponding author.
E-mail address: p.j.m.m.tacx@outlook.nl (P. Tacx).

https://doi.org/10.1016/j.conengprac.2025.106421
Received 20 December 2024; Received in revised form 18 May 2025; Accepted 19 May 2025
Available online 19 June 2025

and Steinbuch (1990), Ljung (2009) and Robel (1989). Methods for computing finite-frequency system norms are described in, e.g., Iwasaki and Hara (2005), Petersson and Löfberg (2014) and Vuillemin, Poussot-Vassal, and Alazard (2012). However, a parametric system description is often not available in full detail in many applications. A parametric system description could be obtained through system identification which however can lead to a high level of user intervention, e.g., the selection of an appropriate model structure, model order, and algorithm, especially for multivariable systems. Model validation techniques have been developed to estimate the $\mathcal{H}_\infty$ norm in Poolla, Khargonekar, Tikku, Krause, and Nagpal (1994) and Smith and Doyle (1992). However, these techniques often result in underestimates of the $\mathcal{H}_\infty$ norm.

The aim of this paper is to combine the advantages of data-driven and full-parametric methods by exploiting local parametric modeling techniques to estimate system norms. By exploiting local smoothness, these local parametric methods can be used to estimate the transient, at-grid, and inter-grid behavior which reduces experiment time and improves the estimation quality without the complexities of full-parametric identification. These methods are successfully applied in several applications, see, e.g., Evers, de Jager, and Oomen (2018), Pintelon, Schoukens, Vandersteen, and Barbé (2010a, 2010b), Tacx, Habraken, Witvoet, Heertjes, and Oomen (2024) and Voorhoeve, van der Maas, and Oomen (2018). However, these approaches do not consider the inter-grid system behavior and solely focus on improving the estimate for the at-grid system behavior. Alternatively, Gaussian Processes can further enhance the estimation quality for frequency response estimates, as demonstrated in Hallemans, Pintelon, Joukovsky, Peumans, and Lataire (2022), and can be used to estimate the inter-grid system behavior. However, this approach requires significant computational effort, particularly for multivariable systems. Therefore, this paper adopts local parametric models. The key idea in this paper is to evaluate the local parametric description to estimate the inter-grid behavior. The potential of these local models for estimating the $\mathcal{H}_\infty$ was investigated previously in Geerardyn and Oomen (2017) but this method was limited to SISO systems and relied on a pragmatic selection of the frequency grid to estimate the local peak norms. This may lead to underestimation of system norms, in particular for $\mathcal{H}_\infty$ norms, in case of lightly-damped resonances. An additional advantage of local parametric methods is that these can be used to provide variance estimates of the obtained frequency response results (Pintelon et al., 2010b). However, this paper is focused only on the nominal value.

Despite the substantial progress in the literature, current methods for estimating system norms may lead to inaccurate estimates, require a significant amount of measurement time, or demand a high level of user intervention. This paper proposes an approach to accurately and reliably estimate the finite-frequency and global $\mathcal{H}_2$ and $\mathcal{H}_\infty$ norm with a limited amount of data. The proposed approach includes estimating the finite-frequency $\mathcal{H}_2$ and $\mathcal{H}_\infty$ norms. The main contributions of this paper are:

C1 an approach that exploits local parametric modeling techniques for estimating the global and finite-frequency

- C1.1 $\mathcal{H}_2$ norm.
- C1.2 $\mathcal{H}_\infty$ norm.

C2 the application of the proposed method in

- C2.1 a simulation case study.
- C2.2 an experimental case study.

The method proposed in this paper estimates the system norms by calculating finite-frequency norms of the local parametric models within their respective frequency intervals. For $\mathcal{H}_\infty$ norm estimation, an algorithm is introduced to compute the finite-frequency $\mathcal{L}_\infty$ norm of these models. Traditional methods calculate peak values over infinite-frequency intervals using weighting filters to highlight specific regimes, but these weighting filters complicate the process and only approximate the problem. By employing the generalized KYP lemma, the computation is reformulated into a finite-dimensional Linear Matrix Inequality (LMI)-based feasibility test, enabling accurate and efficient computation of the finite-frequency $\mathcal{H}_\infty$ norms (Iwasaki & Hara, 2005; Iwasaki, Meinsma, Fu, et al., 2000; Pipeleers & Vandenberghe, 2011). Alternatively, the $\mathcal{H}_\infty$ norm can be estimated analytically for single-input–single-output systems. This can potentially be extended to multivariable systems through symbolic toolbox packages. For $\mathcal{H}_2$ norm estimation, local finite-frequency $\mathcal{H}_2$ norms are computed for each model in its frequency interval. Parametric methods could be employed to compute the local finite-frequency $\mathcal{H}_2$ norm of the local parametric models, see, e.g., Gawronski (2004) and Van Loan (1978). However, these methods either require stable local models or local models with real-valued coefficients. Since these models are often parameterized with complex-valued coefficients, these requirements restrict the modeling flexibility which is not desirable. For this reason, the integral is computed numerically using a cumulative trapezoidal integration scheme. This method is known to yield accurate estimates when a sufficiently dense grid is used. It is important to emphasize that the considered grid operates along the domain of the local parametric models and is therefore substantially denser than the sparsely spaced DFT grid, without requiring additional data or experiments. As a result, it enables significantly more accurate estimates compared to traditional system norm estimation methods based on spectral analysis, as seen in, e.g., Anderson et al. (1991) and Van de Wal et al. (2002).

The novelty in this paper lies in the derivation and application of a method for estimating $\mathcal{H}_2$ and $\mathcal{H}_\infty$ norms of multivariable systems which has not been previously published in its full generality. This paper extends to the previous result in Tacx and Oomen (2021) by providing, a method for estimating $\mathcal{H}_2$ norms, an extended and revised derivation of the system norm estimation method, and the application in an extensive experimental and simulation case study.

The outline of this paper is as follows. In Section 2, the system norms and the problem considered in this paper are introduced. In Section 3, the local modeling techniques that are used for estimating the system norms are introduced. In Section 4, the method for estimating the $\mathcal{H}_2$ norm is proposed. In Section 5, the method for estimating the $\mathcal{H}_\infty$ norm is proposed. In Section 6, the proposed techniques are demonstrated in a simulation case study. In Section 7, the proposed techniques are applied in an experimental case study. In Section 8, the conclusions of this paper are formulated.

The following notation is used throughout. For a matrix A, the maximum singular value is given by $\bar{\sigma}(A)$. The transpose and complex conjugate transpose of a matrix A is denoted by $A^\top$ and A^* respectively. The trace of a matrix A is defined as $\mathrm{tr}(A)$.

2. Problem formulation

2.1. System norms

In this paper, a frequency domain-based approach is pursued to determine the system norms of a multivariable linear time-invariant system $G_o \in \mathbb{C}^{n_y \times n_u}$, where n_y denotes the number of outputs and n_u the number of inputs, as indicated in Fig. 1. Throughout, the generalized frequency variable is denoted by ξ which becomes when formulated in continuous time $\xi = j\omega$ with $\omega \in \mathbb{R}$, and in the discrete time $\xi = e^{j\omega T_s}$ with $\omega \in \left[0, \frac{\pi}{T_s}\right]$, where T_s denotes the sampling time, the latter is used throughout. Consider the frequency domain interpretations of the $\mathcal{H}_2$ and $\mathcal{H}_\infty$ norm.

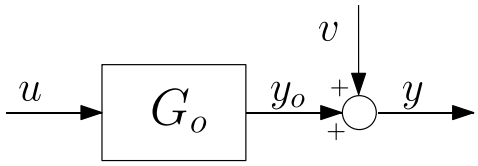

Fig. 1. Linear time invariant system in an open-loop setting with input u, measurement noise v, and undisturbed output y_o and the output y.

Definition 1. Given a multivariable linear time-invariant system G_o. The $\mathcal{H}_\infty$ norm is defined as

$$\gamma = \|G_o\|_\infty = \sup_{\omega\in\Omega} \bar{\sigma}\left(G_o(\xi)\right) \tag{1}$$

where Ω denotes the frequency range which is formulated in discrete time as $\Omega = \left[0, \frac{\pi}{T_s}\right]$.

Definition 2. Given a multivariable linear time-invariant system G_o. The $\mathcal{H}_2$ norm is defined as

$$\mu = \|G_o\|_2 = \sqrt{\frac{1}{2\pi}\int_\Omega \operatorname{tr}\left(G_o^*(\xi)G_o(\xi)\right) d\omega} \tag{2}$$

where Ω denotes the frequency range which is formulated in discrete time as $\Omega = \left[0, \frac{\pi}{T_s}\right]$.

A key issue arises from the fact that no explicit access to the parametric system description is provided. As a consequence, only experimental input–output data is available.

Remark 1. Some applications require to focus on a specific finite-frequency range. Consider the finite-frequency counterparts of the $\mathcal{H}_2$ and $\mathcal{H}_\infty$ norm. Throughout this paper, unless stated otherwise, the global system norms in Definitions 1 and 2 are considered. However, it is important to note that the proposed methods can be readily used to estimate the finite-frequency norms by replacing the infinite frequency range Ω in (1) and (2) with a specific finite-frequency range Ω_{ff}. This choice is made to enhance the readability of the results by avoiding introducing additional notation for the finite-frequency case.

2.2. Spectral analysis

Consider the discrete signal $u(n)$, $n = 0, 1, \ldots, N-1$. The Discrete Fourier Transform (DFT) of $u(n)$ is defined as

$$U(k) = \frac{1}{\sqrt{N}}\sum_{n=0}^{N-1} u(n)\exp\left(\frac{-i2\pi kn}{N}\right)$$

where $k \in \{1, \ldots, N\}$ denotes the kth DFT bin.

In Fig. 1, the linear time-invariant system G_o is depicted, where $u(n)$ represents the input, $y_o(n)$ the noiseless output, $y(n)$ represents the output, and $v(n)$ corresponds to the noise at the output. The noise $v(n)$ is colored and characterized by $V(k) = H(\xi_k)E(k)$, where $H(\xi_k)$ serves as the noise model and $e(n)$ is a zero-mean Gaussian white noise signal. The response to the discrete input $u(n)$ is given by (Pintelon et al., 2010b; Tacx et al., 2024)

$$Y(k) = G_o(\xi_k)U(k) + V(k) + T(\xi_k), \tag{3}$$

where $Y(k)$ denotes the output response and $T(\xi_k)$ denotes the transient component of the response. Here, ξ_k is the frequency variable associated with DFT-bin k, which translates to $\xi_k = j\omega_k$ in the Laplace domain and $\xi_k = e^{j\omega_k T_s}$ in the Z-domain.

The traditional approach to estimate the system norm of $G_o(\xi_k)$ is based on spectral analysis. This method relies on the finite number of DFT lines that are available in a frequency response estimate. To obtain the frequency response function estimate, n_u independent experiments are conducted. The resulting spectra are stacked in the matrices $U_M(k)$ and $Y_M(k)$. Additionally, averaging and an appropriate window function can be used to improve the quality of the estimate. By multiplying the resulting averaged cross-spectra with the inverse of the averaged auto-spectra, the frequency response function is estimated

$$\hat{G}_{\text{SA}}(\xi_k) = \left[Y_M(k)\overline{U_M}(k)\right]\left[U_M(k)\overline{U_M}(k)\right]^{-1}. \tag{4}$$

The $\mathcal{H}_2$ and $\mathcal{H}_\infty$ norms defined in (2) and (1) are approximated as

$$\tilde{\mu}_{\text{FRF}} = \sqrt{\frac{1}{2\pi}\sum_{k=1}^{N-1} \operatorname{tr}\left(\hat{G}_{\text{SA}}^*(\xi_k)\hat{G}_{\text{SA}}(\xi_k)\right)\left(\xi_{k+1} - \xi_k\right)} \tag{5}$$

and

$$\tilde{\gamma}_{\text{FRF}} = \max_{k\in\{1,\ldots,N-1\}} \bar{\sigma}\left(\hat{G}_{\text{SA}}(\xi_k)\right). \tag{6}$$

This means that direct inspection of the FRF data only gives access to $\tilde{\mu}_{\text{FRF}}$ and $\tilde{\gamma}_{\text{FRF}}$ which do not necessarily coincide with the true system norms γ and μ for two reasons.

1. The transients, in addition to the noise contribution $V(k)$, lead to an estimation error in the frequency response estimate, i.e.,

   $$G_o(\xi_k) - \hat{G}_{\text{SA}}(\xi_k) = T(\xi_k)U^{-1}(k) + V(k)U^{-1}(k).$$

   This means that the system norm estimations are biased due to the presence of the transient contribution in the frequency response estimate (4). This estimation bias can be substantial for systems with large time constants, such as thermal systems, see, e.g., Evers et al. (2018).
2. Due to limited experimentation time, the system response is only estimated at a finite discrete frequency grid. Hence, the finite frequency resolution may not be sufficiently dense to capture the dynamics of the system, especially for lightly-damped systems with resonant behavior.

The use of spectral analysis-based system norm estimation methods in (5) and (6) are often used in practical applications, see, e.g., Anderson et al. (1991) and Van de Wal et al. (2002). The combination of the unmodeled transient behavior and the unmodeled inter-grid system behavior could potentially lead to a system norm estimation bias. The main contribution of this paper is to estimate the transient and inter-grid behavior without the need for a global parametric model. Instead, the $\mathcal{H}_2$ and $\mathcal{H}_\infty$ norms are obtained using local parametric modeling techniques that are valid over a finite-frequency interval.

3. Local modeling for $\mathcal{H}_2$-norm and $\mathcal{H}_\infty$-norm estimation

Accurate estimation of the transient and the inter-grid behavior is crucial to obtain an accurate and reliable estimate of the $\mathcal{H}_2$ and $\mathcal{H}_\infty$ norm. This section aims to exploit local modeling techniques to estimate the transient and the inter-grid behavior.

3.1. Transient elimination

The main mechanism of local modeling approaches is to exploit the local smoothness of a system by introducing a local parametric model of the system and the transient (McKelvey & Guérin, 2012; Pintelon et al., 2010a; Tacx et al., 2024; Voorhoeve et al., 2018). These models are estimated by introducing a window around the kth DFT bin, i.e.,

$$r \in \left[-N_W, \ldots, N_W\right] \in \mathbb{Z},$$

where the window size N_W determines the size of the DFT window on which the local parametric models are estimated. This parameter is selected by the control engineer. The local model at bin k can be expressed as

$$Y(k+r) = \tilde{G}_k(r)U(k+r) + \tilde{T}_k(r), \tag{7}$$

where $\tilde{G}_k(r)$ and $\tilde{T}_k(r)$ denote the kth local model and transient models, respectively.

3.2. Parametrization & algorithm

The local models $\tilde{G}_k(r)$ are described by the left matrix fraction description (LMFD)

$$\tilde{G}_k(r) = D_k^{-1}(r,\theta)N_k(r,\theta), \qquad \tilde{T}_k(r) = D_k^{-1}(r,\theta)M_k(r,\theta). \tag{8}$$

Here, $D_k(r)$, $N_k(r)$, and $M_k(r)$ are polynomial matrices with respective orders N_D, N_N, and N_M, as outlined in Voorhoeve et al. (2018). A large number of LMFD parametrizations exist in the literature, see, e.g., Voorhoeve et al. (2018) for an extensive overview and comparison of these parametrizations for local parametric methods, i.e., local rational method (LRM). In this paper the full polynomial parametrization is employed because it enables to describe and estimate accurate local parametric models for a relatively large range of systems while using a limited number of parameters, supporting a small N_W which supports the mitigation of estimation bias and a sufficient degree of averaging (Voorhoeve et al., 2018). In addition, selecting low model orders also avoids pole-zero cancellations leading to potentially sharp resonances. Moreover, setting $N_D = 0$ adapts the method to the local polynomial method.

The multivariable local models are estimated through the linear least-squares optimization for all k

$$\hat{\theta}(k) = \arg\min_{\theta} \sum_{r=-N_W}^{N_W} \Big\| D_k(r,\theta)Y(k+r) - N_k(r,\theta)U(k+r) - M_k(r,\theta)\Big\|_2^2. \tag{9}$$

This optimization, which resembles the Levy method, is computationally efficient and typically sufficiently accurate in practice (Levy, 1959; Voorhoeve et al., 2018). However, the specific structure may lead to an estimation bias. This bias can be mitigated by employing an iterative version of (9) which introduces a significant additional computational cost that typically leads to only a limited improvement in the quality of the estimation (Voorhoeve et al., 2018).

The techniques presented in this paper are based on an open-loop configuration as described in (3). Nevertheless, the modeling framework defined by (7) can be extended to accommodate closed-loop systems, as demonstrated in, e.g., Pintelon and Schoukens (2012).

3.3. Local models for norm estimation

The key idea is to employ local parametric models to estimate the inter-grid behavior. An important step is to employ the real variable r on the continuous and real finite-frequency interval $r \in \lambda$ which enables to evaluate the local models on and in-between the DFT grid. The domain λ is a continuous segment of the real axis

$$\tilde{G}_k(r), \quad r \in \lambda, \qquad \lambda = \left\{ r \in \mathbb{R} \,\middle|\, -r_\Delta \le r \le r_\Delta, r_\Delta \ge 0.5 \right\}. \tag{10}$$

where $\tilde{G}_k(r)$ denotes the kth local parametric model that depends on the real variable r which is part of the validity range λ. The parameter r_Δ is a parameter that is determined by the control engineer which determines the validity range λ of the local parametric models. If the validity range is $r_\Delta > 0.5$, the local parametric models overlap each other. For $r_\Delta = 0.5$, the local parametric models form a piece-wise function. To improve the readability of this paper, a validity range $r_\Delta = 0.5$ is used throughout this paper. Nevertheless, the results proposed in this paper can be extended to accommodate the situation where $r_\Delta > 0.5$.

A complicating aspect arises from the fact that the local parametric models operate along the λ domain which is a finite segment of the DFT axis, i.e., real axis, while the integration in the $\mathcal{H}_2$-norm definition takes place along the frequency variable ω. The frequency variable ω is related to the λ domain through

$$k + r = f_{\omega\mapsto k+r}(\omega), \qquad f_{\omega\mapsto k+r}(\omega) = \frac{NT_s}{\pi}\omega. \tag{11}$$

The function $f_{\omega\mapsto k+r}(\omega)$ in (11) provides a frequency domain interpretation of the continuous description of the local parametric models. The transformations of the frequency variable ω to Laplace domain and Z-domain can be considered as Möbius transformations, as indicated in Fig. 2.

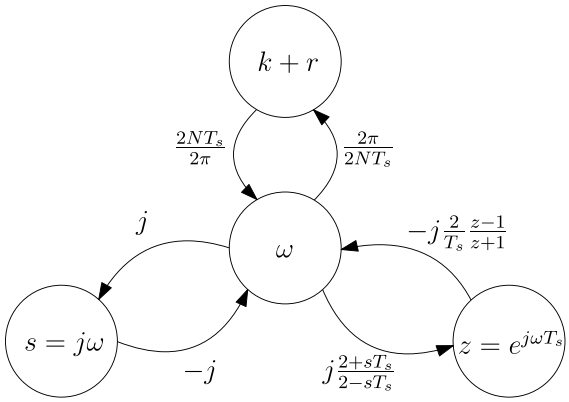

Fig. 2. Diagram indicating the Möbius transformations that connect the real (DFT) axis which is used by local parametric models, Laplace and Z-domain.

The key idea of this paper is to incorporate the inter-grid behavior of local parametric models within their respective frequency intervals to enhance the estimation of the $\mathcal{H}_\infty$ and $\mathcal{H}_2$ norms. This objective fundamentally differs from existing approaches in the literature (McKelvey & Guérin, 2012; Pintelon et al., 2010a; Tacx et al., 2024; Voorhoeve et al., 2018), where local models are used solely to estimate the at-grid frequencies, and hence mainly aiming to improve the quality of the frequency response function estimate.

4. $\mathcal{H}_2$-norm estimation

The main idea in this paper is to exploit the local parametric models introduced in Section 3 to estimate system norms. In this section, these local parametric models are used to estimate the finite-frequency $\mathcal{H}_2$ norm, which constitutes Contribution C1.1. The approach focuses on estimating the global norm by computing the local finite-frequency norms of the individual local parametric models, i.e.,

$$\|G_o\|_2^2 = \sum_{k=0}^{N-1} \mu_{\text{loc},k}^2$$

where $\mu_{\text{loc},k}$ denotes the local finite-frequency norm of the kth local parametric model.

The local finite-frequency norm of the kth local parametric model is defined as

$$\mu_{\text{loc},k} = \int_{-r_\Delta}^{r_\Delta} \operatorname{tr}\left(\tilde{G}_k(r)\tilde{G}_k^*(r)\right) f'_{\omega\mapsto r}\, dr = \int_{-r_\Delta}^{r_\Delta} \operatorname{tr}\left(\tilde{G}_k(r)\tilde{G}_k^*(r)\right) \frac{NT_s}{\pi}\, dr$$

The term $f'_{\omega\mapsto r}$ refers to the derivative of $f_{\omega\mapsto r}$ with respect to the frequency variable ω. This term follows from the reverse chain rule, i.e., the conversion from the λ domain to the frequency variable ω. Analytic solutions to this integral only exist in specific cases, e.g., for $N_D = 0$, the polynomial parametrization. Dedicated finite-frequency $\mathcal{H}_2$-norm techniques such as, e.g., Petersson and Löfberg (2014) and Vuillemin et al. (2012), require stable local parametric models or real-valued

coefficients, which limits the generality of the results. For this reason, the integral is computed numerically using a cumulative trapezoidal integration scheme. This method is known to yield accurate estimates when a sufficiently dense grid is used along the real axis segment λ. It is important to emphasize that the considered grid operates along this real axis segment λ and is therefore substantially denser than the sparsely spaced DFT grid, without requiring additional data or experiments. As a result, it enables significantly more accurate estimates compared to traditional system norm estimation methods based on spectral analysis, as seen in, e.g., Anderson et al. (1991) and Van de Wal et al. (2002).

5. $\mathcal{H}_\infty$-norm estimation

The global $\mathcal{H}_\infty$ norms are estimated by computing the finite-frequency $\mathcal{L}_\infty$ norm of each local parametric model within its respective frequency interval. This section develops a method for accurately estimating these finite-frequency $\mathcal{L}_\infty$ norms, which constitutes Contribution C1.2.

5.1. $\mathcal{H}_\infty$ norm estimation: Approach

Estimating the $\mathcal{H}_\infty$ norm involves two main steps. First, the finite-frequency $\mathcal{L}_\infty$ norms of the individual local parametric models are computed as

$$\gamma_k = \sup_{r\in\lambda} \bar{\sigma}\left(\tilde{G}_k(r)\right), \tag{12}$$

where $\tilde{G}_k$ denotes the kth local model.

Using these local estimates, the global $\mathcal{H}_\infty$ norm is determined by taking the maximum finite-frequency $\mathcal{L}_\infty$ norm across all local parametric models

$$\|G_o\|_\infty^2 = \tilde{\gamma} = \max_k \gamma_k.$$

Thus, accurately computing the finite-frequency $\mathcal{L}_\infty$ norm for each local model is crucial for obtaining an accurate estimate of the global $\mathcal{H}_\infty$ norm. In the following section, an algorithm is introduced that leverages the local parametric description to compute the local norm accurately.

5.2. Finite-frequency $\mathcal{L}_\infty$-norm algorithm

This section introduces a method for determining the finite-frequency $\mathcal{L}_\infty$ norm of the local parametric models. The following theorem presents an important result in the development of the algorithm by converting the estimation problem to a finite-dimensional LMI by employing the generalized KYP lemma, see, e.g., Iwasaki and Hara (2005). One approach to estimate the peak value in (12) is to check the frequencies $r \in \lambda$ in a finite frequency grid. However, due to resonances, such a pragmatic approach may lead to underestimation of the finite-frequency $\mathcal{L}_\infty$ norm. To this end, an approach is developed that leads to a new algorithm that enables the computation of the finite-frequency $\mathcal{L}_\infty$ norm of local parametric models based on a finite-dimensional LMI.

Theorem 1. *Let $\tilde{G}_k$ be a local model of the form (8) with validity range λ according to (10). Suppose that $\tilde{G}_k$ has the following form*

$$\tilde{G}_k(r) = C\left(rI - A\right)^{-1}B + D \tag{13}$$

where $A \in \mathbb{C}^{n_x\times n_x}$, $B \in \mathbb{C}^{n_x\times n_u}$, $C \in \mathbb{C}^{n_y\times n_x}$ and $D \in \mathbb{C}^{n_y\times n_u}$. Then, the following statements are equivalent.

1. *The finite-frequency $\mathcal{L}_\infty$ norm of $\tilde{G}_k(\xi)$ on the domain λ is bounded by $\tilde{\gamma}_k$*

$$\sup_{r\in\lambda} \bar{\sigma}\left(\tilde{G}_k(\xi)\right) < \tilde{\gamma}_k. \tag{14}$$

2. *There exist a $P, Q \in \mathbb{H}_n$ such that*

$$Q \succ 0$$

$$F(\gamma_k) = \begin{bmatrix} A & B \\ I & 0 \end{bmatrix}^* (\Phi \otimes P + \Psi \otimes Q) \begin{bmatrix} A & B \\ I & 0 \end{bmatrix} + \begin{bmatrix} C & D \\ 0 & I \end{bmatrix}^* \begin{bmatrix} I & 0 \\ 0 & -\tilde{\gamma}_k^2 I \end{bmatrix} \begin{bmatrix} C & D \\ 0 & I \end{bmatrix} \prec 0 \tag{15}$$

with

$$\Phi = \begin{bmatrix} 0 & j \\ -j & 0 \end{bmatrix}, \Psi = \begin{bmatrix} -1 & 0 \\ 0 & r_\Delta^2 \end{bmatrix}. \tag{16}$$

The proof is presented in Appendix.

Essentially, Theorem 1 enables to reformulate the finite-frequency $\mathcal{L}_\infty$-norm bound on the domain λ into a finite-dimensional LMI in (15) through the generalized KYP lemma. For details regarding the generalized KYP lemma, see, e.g., Iwasaki and Hara (2005), Iwasaki et al. (2000). The rational local parametric models that are considered in this paper can be trivially rewritten into the state-space format in (13) in Theorem 1. This includes the local polynomial case, i.e., $N_D = 0$.

The key idea in this paper is to exploit the result presented in Theorem 1 by considering the finite-dimensional feasibility test in matrices P and Q for a fixed finite-frequency $\mathcal{L}_\infty$ norm bound $\tilde{\gamma}_k$. The local bound γ_k in (12) is then computed iteratively through a bisection algorithm applied to this bound as demonstrated in the following algorithm.

Algorithm 1 (*Finite-Frequency $\mathcal{L}_\infty$-norm Algorithm*)**.** Let $\tilde{G}_k(r)$ be the local parametric model with validity range λ, and let $F(\gamma_k)$ be the feasibility condition as defined in (15). The finite-frequency $\mathcal{L}_\infty$ norm bound γ_k is computed iteratively using the following bisection algorithm.

1. **Initialization:** Determine an initial interval $[\gamma_{l,1}, \gamma_{u,1}]$, where $\gamma_{l,1}$ denotes the lower bound and $\gamma_{u,1}$ denotes the upper bound, such that:
   - $F(\gamma_{l,1})$ is infeasible (i.e., does not satisfy (15)).
   - $F(\gamma_{u,1})$ is feasible (i.e., satisfies (15)).

   Set the iteration counter $i = 1$.
2. **Iteration:** Until the termination, perform the following steps:
   - Compute the midpoint $\gamma_{m,i} = \frac{\gamma_{l,i}+\gamma_{u,i}}{2}$.
   - Check the feasibility of $F(\gamma_{m,i})$:
     - If $F(\gamma_{m,i})$ is feasible, update $\gamma_{u,i+1} = \gamma_{m,i}$.
     - Otherwise, update $\gamma_{l,i+1} = \gamma_{m,i}$.
   - Increment $i = i + 1$.
3. **Termination:** The algorithm converges when $|\gamma_{u,i} - \gamma_{l,i}|$ is below a predefined tolerance ϵ, at which point the final estimate is given by

$$\gamma_k = \frac{\gamma_{l,i} + \gamma_{u,i}}{2}. \tag{17}$$

In this paper, the initial interval in Algorithm Algorithm 1 is determined based on the estimate of the local parametric models, with specific considerations outlined in the simulation and experimental case studies. If the initial interval is found to be either entirely feasible or infeasible, it can be appropriately adjusted. The key idea in this paper is to employ Algorithm Algorithm 1 for the accurate computation of the finite-frequency $\mathcal{L}\infty$ norm of each local parametric model at the respective DFT bin k, thereby enabling accurate and reliable estimation of the global $\mathcal{H}\infty$ norm.

6. Simulation case study

In this section, the methods for estimating the $\mathcal{H}_\infty$ and $\mathcal{H}_2$ norms are applied in a simulation case study which constitutes Contribution C2.1.

6.1. Simulation description

The case study considers a mechanical model based on the modal form, i.e.,

$$G(s) = \sum_{i=1}^{N} \phi_i \frac{1}{s^2 + 2\zeta_i\omega_i s + \omega_i^2} \phi_i^\top$$

where, ϕ_i, ζ_i, ω_i, and N denote the ith mode shape vector, damping constant, eigenfrequency, and the number of modes respectively. In this case study, a two-input–two-output system is considered with two mechanical modes, i.e. $N = 2$. In Fig. 3, an element-wise Bode magnitude plot of the considered system is depicted. The continuous time system is simulated in a discrete form based on the zero-order hold function and a sampling frequency of 2048 Hz. Experiments are conducted in an open-loop setting as indicated in Fig. 1. Both inputs are simultaneously excited by two independent white Gaussian noise signals with a unit variance. The output disturbance is white Gaussian noise with a variance selected such that the signal-to-noise ratio (SNR) at both outputs is 10.

Traditionally, the spectral analysis method is used to estimate the frequency response function and system norms in practice. The spectral analysis method cannot estimate a multivariable frequency response function from a single experiment unless constraints are imposed on the spectral content of the input signal. In sharp contrast, local parametric modeling techniques only require a single experiment, independent of the number of inputs through smoothness assumptions, see, i.e., Pintelon and Schoukens (2012). For the spectral analysis method, therefore, n_u independent experiments are required and the results are averaged by subdividing the input and output signals into segments $\frac{N}{n_S}$

$$\left[x(n)^{\langle j \rangle}\right]^i = x\left((i-1)n_S + n\right)$$

where $x(n)^{\langle j \rangle}$ is equal to the input $u(n)^{\langle j \rangle}$ and $y(n)^{\langle j \rangle}$ of the jth experiment respectively with $i \in \{1, \dots, n_S\}$, $j \in \{1, \dots, n_u\}$ and $n \in \{0, \dots, \frac{N}{n_S - 1}\}$. The frequency domain counterparts are obtained by means of the DFT and are denoted $\left[U(k)^{\langle j \rangle}\right]^i$ and $\left[Y(k)^{\langle j \rangle}\right]^i$. To reduce leakage, the segments could be windowed using an appropriate windowing function, e.g., Hann window (Pintelon & Schoukens, 2012). The frequency resolution is $\frac{2\pi n_S n_u}{N T_s}$. To compute the frequency response function, the input and output vectors are rearranged to a matrix

$$U_M(k) = \frac{1}{n_S} \sum_{i=1}^{n_S} \left[\left[U(k)^{\langle 1 \rangle}\right]^i \dots \left[U(k)^{\langle n_u \rangle}\right]^i \right],$$

$$Y_M(k) = \frac{1}{n_S} \sum_{i=1}^{n_S} \left[\left[Y(k)^{\langle 1 \rangle}\right]^i \dots \left[Y(k)^{\langle n_u \rangle}\right]^i \right].$$

The frequency response function is estimated in (4). It is clear that the inverse in (4) leads to a condition on the excitation design since the matrix U_M should be regular. In practice, this means that n_u independent experiments with n_u different realizations of the noisy input signal suffice.

Note that for a constant total measurement time, the parameter n_S decreases the frequency resolution but improves the transient leakage error and the noise rejection. Also, the measurement time scales with the number of inputs n_u. Thus, for a constant measurement time, the frequency resolution decreases with the number of inputs n_u. In sharp contrast, the local rational method requires only a single experiment, independent of the number of inputs. This is a key advantage of the local parametric method compared to traditional spectral analysis methods, especially for multivariable systems. The input signal is required to be sufficiently rough in order to estimate the local parametric models. Extensive practical experience and results in the literature, e.g., Tacx et al. (2024) and Voorhoeve et al. (2018), confirm that this requirement is usually fulfilled by independently generated white Gaussian noise signals or independently generated multi-sine signals. For more details on the (optimal) design of the input signals see, e.g., Dirkx, van de Wijdeven, and Oomen (2020).

The aim is to estimate the finite-frequency $\mathcal{H}_\infty$ and $\mathcal{H}_2$ norms in Definitions 1 and 2 by considering a finite-frequency range

$$\Omega_{\text{ff}} = [10, 100] \text{ Hz}.$$

To obtain the highest frequency resolution, the data is not averaged, i.e., $n_S = 1$. Local rational models are considered instead of local polynomial models which leads to substantially more accurate results (Geerardyn & Oomen, 2017; Voorhoeve et al., 2018). The full polynomial form is selected as this parametrization is sufficiently rich for a limited model order. The width of the local rational models should be selected in view of the roughness of the data.

Typically, selecting a relatively small width N_W is preferable to avoid bias caused by excessive smoothing of system dynamics. However, the minimum required width depends on the number of parameters to be estimated, which in turn depends on the model orders $N_D = 4$, $N_N = 4$, $N_M = 4$ and the number of inputs n_u and outputs n_y. Importantly, this relation is inherently tied to the considered model parametrization, e.g., full polynomial, common denominator, polynomial, and is therefore not stated explicitly to preserve the generality of the presented results. Also, this dependency is not specific to the inter-grid approach proposed in this paper but applies more broadly to local model estimation methods in general. Additionally, avoiding pole-zero cancellations supports the use of these relatively low model orders. Extensive experimental experience further indicates that slight variations in these orders do not significantly affect the norm estimation results. To enhance conciseness, such parameter variations are not included in this paper, see, e.g., Pintelon et al. (2010b), Verbeke and Schoukens (2019) and Voorhoeve et al. (2018) for further theoretical considerations regarding the selection of minimal frequency width and model orders.

The finite-frequency interval of the local parametric models in (10) is set to $r_\Delta = 0.5$. The initial estimate of the finite-frequency $\mathcal{L}_\infty$ norm computation is selected based on the at-grid frequency response estimate. Specifically, the lower bound is selected by taking the upper local at-grid estimate, and the upper bound is selected to be a hundred times larger. In case the upper bound turns out to be invalid, it is adjusted accordingly.

6.2. Results

First, the results are studied for a fixed experiment length of 1024 samples, i.e., 0.5 s. The Bode magnitude plot in Fig. 3 shows that the traditional spectral analysis-based approach leads to unreliable estimates of the frequency-response function, due to the noise and transient leakage. In sharp contrast, the local rational modeling approach accurately matches the true system. Similarly, the singular value plot in Fig. 4 confirms that compared to the spectral analysis method, the local rational models enable accurate results with a limited amount of data. Note that since the total experiment length is fixed, the frequency resolution of the spectral analysis method is $n_u = 2$ times smaller.

Table 1 depicts the results of the finite-frequency $\mathcal{H}_\infty$ and $\mathcal{H}_2$ estimates. Clearly, the spectral analysis-based method leads to inaccurate system norm estimates. The poor estimation quality of the finite-frequency $\mathcal{H}_\infty$ norm is mainly attributed to the limited frequency resolution of the DFT grid. Note that the resolution is $n_u = 2$ times smaller compared to the DFT grid considered by the local rational models. The poor estimation quality of the finite-frequency $\mathcal{H}_2$ norm is mainly caused by the limited estimation quality at higher frequencies, due to the transient leakage error. In sharp contrast, the method proposed in this paper includes the transient and the inter-grid behavior. This enables accurate estimation of the finite-frequency system norms.

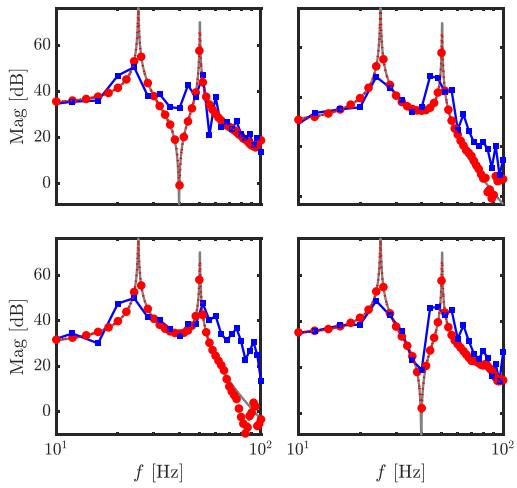

Fig. 3. Simulation case study. Element-wise Bode magnitude plot of the true system G_o (▪▪▪▪), spectral analysis estimate (▬■▬) and interpolated local rational method (▬●▬). The results are based on an experiment with a total length of 1024 samples. The plot reveals accurate at-grid and inter-grid properties and efficient usage of data since the spectral analysis estimate is considerably less accurate. In addition, the Bode plot illustrates that for an equal total experiment length, the grid density of the spectral analysis estimate is at least $n_u = 2$ times smaller.

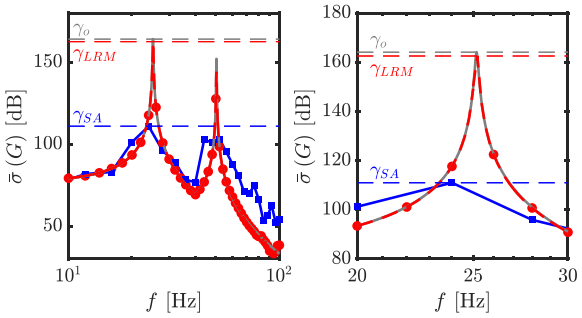

Fig. 4. Simulation case study. Peak singular values plot (left plot depicts the full frequency grid and right plot depicts a closeup) based on the frequency response function of the true system G_o (▬), spectral analysis estimate (▬■▬) and interpolated local rational method (▬●▬). The finite-frequency $\mathcal{H}_\infty$ estimate γ_{LRM} based on the local modeling techniques (▬ ▬) almost coincides with the true value γ_o (▬ ▬). In sharp contrast, the spectral analysis-based estimate γ_{SA} (▬ ▬) leads to significantly underestimation.

Table 1
Finite-frequency norm estimates based for a total experiment length of 1024 samples based on the spectral analysis method and with the method proposed in this paper, i.e., a local parametric modeling-based approach. The estimated finite-frequency norms confirm accurate estimation with efficient usage of data of the method proposed in this paper.

	SA	LRM	True
$\|G\|_{\Omega_{\text{ff}},\infty}$	139.9	163.8	164.1
$\|G\|_{\Omega_{\text{ff}},2}$	3902	7039	7063

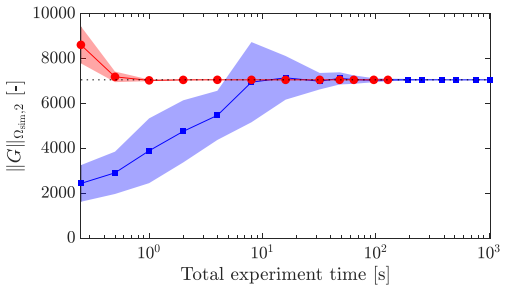

Fig. 5. Simulation case study of the effect of experiment length on the estimation quality of the finite-frequency $\mathcal{H}_2$ norm. The simulation shows that spectral analysis-based estimation (▬■▬) leads to severe underestimation of the finite-frequency $\mathcal{H}_2$ norm for short experiment lengths. The proposed method (▬●▬) is already reliable from experiments that contain almost 100 times less data. The shaded area represent the variance due to the output noise and the transient contribution.

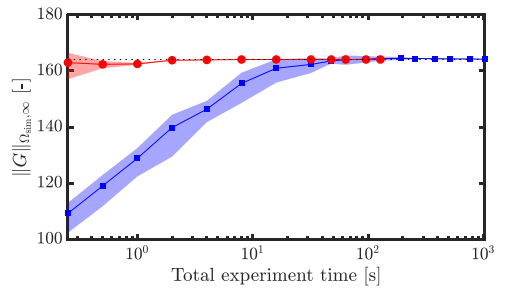

Fig. 6. Simulation case study of the effect of experiment length on the estimation quality of the finite-frequency $\mathcal{H}_\infty$ norm. The simulation shows that spectral analysis-based estimation (▬■▬) leads to severe underestimation of the finite-frequency $\mathcal{H}_\infty$ norm for short experiment lengths. The proposed method (▬●▬) is already reliable from experiments that contain almost 100 times less data. The shaded area represent the variance due to the output noise and the transient contribution.

6.3. Experiment length

In this section, finite-frequency system norm estimation quality is studied for varying experiment lengths. The quality of the finite-frequency system norm estimate strongly depends on the experiment length since it affects the frequency resolution and transient leakage error. The simulations are repeated 50 times with different realizations of the input and output noise. The resulting finite-frequency $\mathcal{H}_\infty$ and $\mathcal{H}_2$ norm estimate, i.e., average and standard deviations, are shown in Figs. 6 and 5.

Figs. 6 and 5 indicate that large experiment lengths are required to obtain a reliable estimate of the finite-frequency system norms for the spectral analysis-based method. In contrast, the local modeling-based approach provides accurate and reliable estimates with a relatively short experiment length. For long experiment lengths, the spectral analysis and local modeling-based methods are similar. Similar to the traditional spectral analysis-based norm estimation methods, no explicit minimum frequency resolution can be provided to obtain accurate estimations of the system norm. However, since in many practical situations, the dynamics are known upfront due to simulations, e.g., finite-element or first-principles models, the dynamics are roughly known upfront based on which a minimum frequency resolution can be estimated. The key benefit of the method proposed in this paper is that substantially less data is required, i.e., 140 times less in this section, compared to the spectral analysis-based methods. In addition, resonances can be modeled with significantly more details.

7. Experimental case study

In this section, the methods for estimating the $\mathcal{H}_\infty$ and $\mathcal{H}_2$ norms are applied in an experimental case study which constitutes Contribution C2.2.

7.1. Setup

The experimental overactuated beam setup is depicted in Fig. 7. The considered system is designed to exhibit out-of-plane flexible dynamic behavior. The system consists of a flexible beam with dimensions $2 \times 20 \times 500$ mm. The system operates in 2 DOFs, one translation, and one rotation. Four degrees of freedom are constrained by wire flexures. Due to the limited out-of-plane stiffness of the beam, the

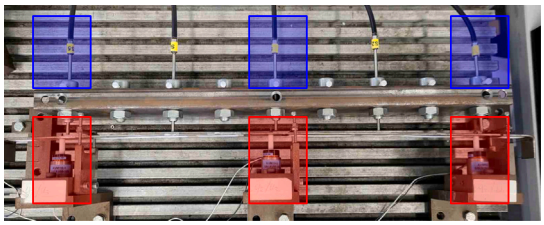

Fig. 7. Experimental overactuated beam setup. Three degrees of freedom are constrained by four vertical wire flexures, and one degree of freedom is constrained by a horizontal wire flexure on the left. The setup is equipped with by three voice coil actuators (■), five position sensors of which three are considered in this paper (■).

system contains a significant number of light-damped flexible modes. The setup is equipped with three Akribis AVM19-5 voice-coil actuators and the position is measured contactless by five Philtec D64-NQ fiberoptic sensors, with a resolution of 1 μm. To facilitate exposition, only the three collocated sensors are considered in the experimental case study. A Beckhoff EtherCAT module is used for data acquisition with a sampling frequency of 2048 Hz.

7.2. Aim

The aim of this study is to estimate the finite-frequency system norms with the method proposed in this paper in the finite-frequency range

$$\Omega_{\text{ff}} = [20, 400] \text{ Hz}.$$

To illustrate the effectiveness of the proposed approach and a parametric true system description of an experimental setup is not available, the results are compared to a benchmark measurement. The spectral analysis-based frequency response measurements are known to provide an accurate estimate of the frequency response for large experiment lengths, which is confirmed by the results in Section 6 and the results in Voorhoeve et al. (2018). For this reason, the results generated by the method proposed in this paper are validated and compared to a long measurement which is processed with spectral analysis. The case study illustrates that the method proposed in this paper provides similar results with significantly less data.

The minimum width of the local parametric models depends on the number of parameters that need to be solved. Therefore, the minimum width is proportional to the parameters N_D, N_N, N_M. The specific orders of LRM have been selected to keep N_W small and leave a sufficient amount of flexibility for the local parametric models, i.e., $N_M = 2$, $N_M = 2$, and $N_M = 2$. In practice, slight to moderate variations in the parametrization orders N_D, N_N, N_M and width N_W do not lead to significant changes in the norm estimation results. To improve the conciseness of the results, these parameter variations are not included in this paper. The finite-frequency interval of the local parametric models in (10) is chosen to be $r_\Delta = 0.5$. Since the considerations of the selection of the local parametric modeling parameters are similar to the simulation results, see Section 6.1 for an overview of the considerations. The initial estimate of the finite-frequency $\mathcal{L}_\infty$ norm computation is selected based on the at-grid frequency response estimate. Specifically, the lower bound is selected by taking the upper local at-grid estimate, and the upper bound is selected to be fifty times larger. In case the upper bound turns out to be invalid, it is adjusted accordingly.

7.3. Results

The validation data for the spectral analysis estimate is defined by $n_u = 3$ independent random-phase multisine signals that are applied to all inputs simultaneously. $M = 30$ different realizations of the input signals are considered, where each realization contains 12 periods. The total experiment time is 4320 s, resulting in a total data length of approximately 10^7 samples. The frequency resolution is 0.25 Hz.

The estimation data is obtained by a single realization of the multisine signal of 30 s and contains 60 periods. The frequency resolution is 2 Hz. Similar to the traditional spectral analysis-based norm estimation methods, no explicit minimum frequency resolution can be provided to obtain accurate estimations of the system norm. However, since in many practical situations, the dynamics are known upfront due to simulations, e.g., finite-element or first-principles models, the dynamics are roughly known upfront, based on which a minimum frequency resolution can be estimated. The key benefit of the method proposed in this paper is that substantially less data is required, i.e., 140 times less in this section, compared to the validation data set.

Table 2
Finite-frequency norm estimates based on the validation experiment with a dense frequency grid and a short experiment that is processed with the method proposed in this paper, i.e., a local parametric modeling-based approach with a significantly shorter experiment and thus a course frequency resolution. The estimated finite-frequency norms confirm accurate estimation with efficient usage of data.

	Validation	LRM
$\|G\|_{\Omega_{\text{ff}},\infty}$ [dB]	40.54	40.78
$\|G\|_{\Omega_{\text{ff}},2}$ [−]	11.14	11.62

The frequency response function estimations based on the validation and estimation data are shown in Figs. 8 and 9. From the element-wise Bode magnitude plot can be concluded that the local rational method accurately matches the spectral analysis-based estimate over the domain Ω_{exp} on the at-grid frequencies. In contrast, at frequencies in the vicinity of 100 Hz, some discrepancies between the validation and estimation estimate can be observed. From practical experience with this setup, this can be attributed to nonlinear effects in the capacitive sensors. Although the estimation data set is significantly smaller, the inter-grid estimate of the local rational models accurately matches the at-grid spectral analysis-based estimates, as shown in Fig. 8.

In addition, in Figs. 10 and 11, the estimation error of the interpolated local rational models with respect to the dense validation data that is processed with spectral analysis is depicted. Also, from this figure, it can be concluded that the method enables excellent interpolation with only a fraction of the data. Near the resonances, the estimation error increases slightly. However, relatively, the error remains small over the entire frequency range.

In Table 2, the finite-frequency norm estimates $\|G_o\|_{\Omega_{\text{exp}},2}$ and $\|G_o\|_{\Omega_{\text{exp}},\infty}$ based on the validation data and estimation data are presented. Clearly, the finite-frequency norms are similar. In Fig. 12, the peak singular values plot is depicted. The local rational method-based approach accurately matches the validation data set. In particular, around the peak singular value, the inter-grid behavior is accurately estimated. The experimental case study illustrates the effectiveness of the proposed method in practice.

8. Conclusions

In this paper, a method is presented for accurate and reliable estimation of the global and finite-frequency $\mathcal{H}_2$ and $\mathcal{H}_\infty$ norm. Traditional methods aim to estimate system norms based on frequency response function estimates. As a result, these methods only consider the finite number of DFT lines which leads to inter-grid errors, and do not consider the transient system behavior. The key step in this paper is to employ local parametric models to take the inter-grid and transient system behavior into account in the system norm estimation procedure.

In Section 3, the local modeling procedure tailored to system norm estimation is introduced. The key idea is to estimate the global system norms through finite-frequency norm computation of the local parametric models in their respective finite-frequency intervals. In

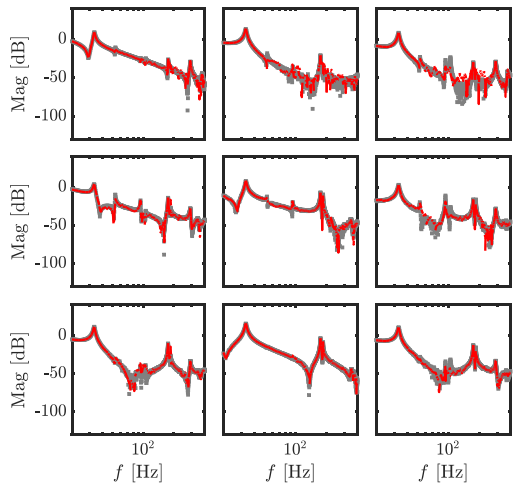

Fig. 8. Experimental case study. Element-wise Bode magnitude plot of the long validation experiment which is processed with spectral analysis (■) and interpolated local rational method estimate based on the estimation data set (—●—). The validity of the local parametric modeling-based approach is confirmed by the validation measurement with the dense frequency grid. The plot reveals excellent interpolation properties and efficient usage of data since the estimation data set is considerably smaller. A close-up for the frequencies in the vicinity of the peak-singular value is depicted in Fig. 9.

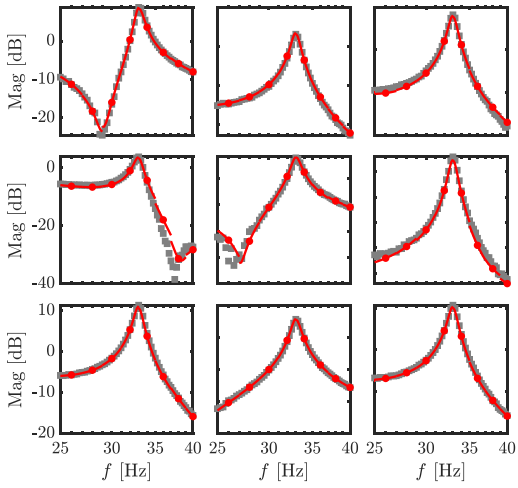

Fig. 9. Experimental case study. Closeup of the element-wise Bode magnitude plot in Fig. 8 of the validation experiment which is processed with spectral analysis (■) and interpolated local rational method (—●—). The validity of the local parametric modeling-based approach is confirmed by the validation measurement at the dense frequency grid.

Section 5, a method is developed to estimate the L_∞ norm of local parametric models through a dedicated LMI-based algorithm which is based on the generalized KYP lemma. The global $\mathcal{H}_\infty$ norm of the system is determined by selecting the largest local L_∞ norm of the local parametric models. The approach to estimate the $\mathcal{H}_2$ norm of local parametric models is presented in Section 4. The local $\mathcal{H}_2$ norm of local parametric models is computed through numerical integration. The global $\mathcal{H}_2$ norm of the system is determined by combining the local $\mathcal{H}_2$ norms of the corresponding local parametric models in their limited frequency interval. Overall, the $\mathcal{H}_2$ norm estimation method leads to accurate results for a sufficiently dense frequency grid.

A simulation case study in Section 6 shows that the method proposed in this paper leads to accurate estimation of the inter-grid system dynamics which leads to accurate system norm estimates. In addition, compared to the traditional spectral analysis-based method,

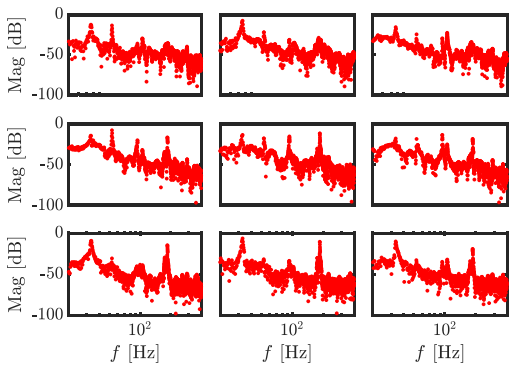

Fig. 10. Experimental case study. Element-wise Bode magnitude plot of the error of the interpolated local parametric models based on the estimation data with respect to the long validation data which is processed with spectral analysis (●). The plot confirms the validity and effectiveness of the proposed approach as it shows excellent interpolation properties. A close-up for the frequencies in the vicinity of the peak-singular value is depicted in Fig. 11.

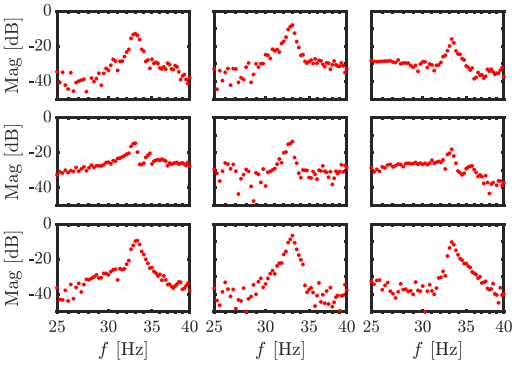

Fig. 11. Experimental case study. Closeup of the element-wise Bode magnitude plot of the interpolation error in Fig. 10 with respect to the validation experiment, which is processed with spectral analysis. The figure confirms the excellent interpolation properties of the proposed approach, enabling accurate system norm estimates.

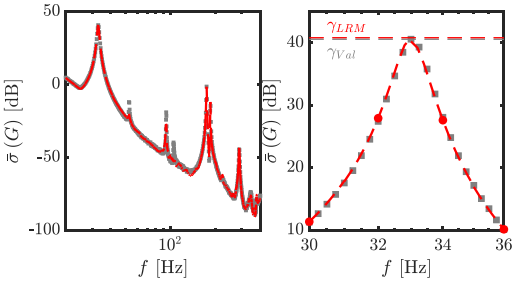

Fig. 12. Experimental case study. Largest singular values (left plot depicts the full frequency grid and right plot depicts a closeup) based on the frequency response function of the validation experiment that is processed with spectral analysis (■) and interpolated local rational method (—●—). The finite-frequency $\mathcal{H}_\infty$-norm based on the validation data (- - -) is similar to the estimation data (- - -), which confirms the effectiveness of the proposed approach.

the local modeling approach leads to accurate and reliable results with significantly less data. An experimental case study in Section 7 demonstrates that the method proposed in this paper can lead to a substantial improvement in the system norm estimation quality with significantly less data.

The proposed system norm estimation method is envisioned to be useful in various control design and analysis problems, including, e.g., robust control and model reduction. Current research focuses on taking the variance estimates which are estimated in local parametric

methods into account in the estimation of the system norm. In addition, current research is also focused on extending the comparison in Sections 6 and 7 to more methods including the method proposed in Vries and Van Hof (1994).

CRediT authorship contribution statement

Paul Tacx: Writing – review & editing, Writing – original draft, Visualization, Validation, Supervision, Software, Resources, Project administration, Methodology, Investigation, Funding acquisition, Formal analysis, Data curation, Conceptualization. **Tom Oomen:** Writing – review & editing, Writing – original draft, Visualization, Validation, Supervision, Software, Resources, Project administration, Methodology, Investigation, Funding acquisition, Formal analysis, Data curation, Conceptualization.

Declaration of competing interest

The authors declare that they have no known competing financial interests or personal relationships that could have appeared to influence the work reported in this paper.

Appendix. Proof of Theorem 1

The following lemma shows the equivalence between (14) and an infinite dimensional frequency domain inequality (FDI).

Lemma 1. *Suppose that $\tilde{G}_k(r)$ is a local rational model which is valid on the domain λ defined by (10). Then, the following statements are equivalent.*

1. *The finite-frequency $\mathcal{L}_\infty$ norm of $\tilde{G}_k(r)$ on the domain λ is bounded by γ_k*

$$\sup_{r\in\lambda} \bar{\sigma}\left(\tilde{G}_k(r)\right) < \gamma_k. \tag{A.1}$$

2. *The FDI*

$$\begin{bmatrix} \tilde{G}_k(r) \\ I \end{bmatrix}^* \Pi \begin{bmatrix} \tilde{G}_k(r) \\ I \end{bmatrix} \prec 0 \tag{A.2}$$

holds for all $r \in \lambda$, where Π contains the finite-frequency $\mathcal{L}_\infty$-norm bound γ_k

$$\Pi = \begin{bmatrix} I & 0 \\ 0 & -\gamma_k^2 I \end{bmatrix}. \tag{A.3}$$

Proof. From the definition of the singular value definition, $\bar{\sigma}^2(\tilde{G}_k(r)) = \lambda_{\max}(\tilde{G}_k(r)\tilde{G}_k^*(r))$ holds for all $r \in \lambda$. From this equality, the inequality in (A.1) is equivalent to $\lambda_{\max}\left(\tilde{G}_k(r)\tilde{G}_k^*(r)\right) < \gamma_k^2 \forall r \in \lambda$. Reformulating based on the fact that $\tilde{G}_k(r)\tilde{G}_k^*(r)$ is symmetric leads to (A.2) with (A.3) being negative definite. This completes the proof that (A.1) is equivalent to (A.2) with (A.3).

The generalized KYP Lemma, e.g., Iwasaki and Hara (2005, Theorem 2) Iwasaki and Hara (2005) and Iwasaki et al. (2000), shows that the FDI in (A.2) and the LMI in (15) specified by the matrices in (16) (Iwasaki & Hara, 2005, Section IV) are equivalent which completes the proof of Theorem 1.

References

Anderson, M. R., Emami-Naeni, A., & Vincent, J. H. (1991). *measures of merit for multivariable flight control: Technical Report*, Systems Control Technology Inc.

Antoulas, A. C. (2005). *Approximation of large-scale dynamical systems*. SIAM.

Boyd, S., Balakrishnan, V., & Kabamba, P. (1989). A bisection method for computing the $\mathcal{H}_\infty$ norm of a transfer matrix and related problems. *Mathematics of Control, Signals, and Systems*, *2*(3), 207–219.

Bruinsma, N., & Steinbuch, M. (1990). A fast algorithm to compute the $\mathcal{H}_\infty$-norm of a transfer function matrix. *Systems & Control Letters*, *14*(4), 287–293.

Devonport, A., Seiler, P., & Arcak, M. (2023). Frequency domain gaussian process models for $\mathcal{H}_\infty$ uncertainties. In *Learning for dynamics and control conference* (pp. 1046–1057). PMLR.

Dirkx, N., van de Wijdeven, J., & Oomen, T. (2020). Frequency response function identification for multivariable motion control: Optimal experiment design with element-wise constraints. *Mechatron.*, *71*, Article 102440.

Evers, E., de Jager, B., & Oomen, T. (2018). Improved local rational method by incorporating system knowledge: with application to mechanical and thermal dynamical systems. *IFAC-PapersOnLine*, *51*(15), 808–813.

Friedman, J. I., & Khargonekar, P. P. (1995). Application of identification in $\mathcal{H}_\infty$ to lightly damped systems: two case studies. *IEEE Transactions on Control Systems Technology*, *3*(3), 279–289.

Gawronski, W. K. (2004). *Advanced structural dynamics and active control of structures*. Springer.

Geerardyn, E., & Oomen, T. (2017). A local rational model approach for $\mathcal{H}_\infty$ norm estimation: With application to an active vibration isolation system. *Control Engineering Practice*, *68*, 63–70.

Hallemans, N., Pintelon, R., Joukovsky, B., Peumans, D., & Lataire, J. (2022). Frf estimation using multiple kernel-based regularisation. *Autom.*, *136*, Article 110056.

Iwasaki, T., & Hara, S. (2005). Generalized KYP lemma: Unified frequency domain inequalities with design applications. *IEEE Transactions on Automatic Control*, *50*(1), 41–59.

Iwasaki, T., Meinsma, G., Fu, M., et al. (2000). Generalized sprocedure and finite frequency KYP lemma. *Mathematical Problems in Engineering*, *6*, 305–320.

Levy, E. (1959). Complex-curve fitting. *IRE Transactions on Automatic Control*, (1), 37–43.

Ljung, L. (2009). Model validation and model error modeling. In *Proceedings 15th IFAC symposium on system identification* (pp. 1435–1440). USA: Santa Barbara.

McKelvey, T., & Guérin, G. (2012). Non-parametric frequency response estimation using a local rational model. *IFAC Proceedings Volumes*, *45*(16), 49–54.

Müller, M. I., & Rojas, C. R. (2019). Gain estimation of linear dynamical systems using thompson sampling. In *The 22nd international conference on artificial intelligence and statistics* (pp. 1535–1543). PMLR.

Oomen, T., van der Maas, R., Rojas, C. R., & Hjalmarsson, H. (2014). Iterative data-driven $\mathcal{H}_\infty$ norm estimation of multivariable systems with application to robust active vibration isolation. *IEEE Transactions on Control Systems Technology*, *22*(6), 2247–2260.

Oomen, T., & Rojas, C. R. (2023). Reset-free data-driven gain estimation: Power iteration using reversed-circulant matrices. arXiv preprint arXiv:2311.12607.

Persson, D., Koch, A., & Allgöwer, F. (2020). Probabilistic h2- norm estimation via gaussian process system identification. *IFAC-PapersOnLine*, *53*(2), 431–436.

Petersson, D., & Löfberg, J. (2014). Model reduction using a frequency-limited H2-cost. *Systems & Control Letters*, *67*, 32–39.

Pintelon, R., & Schoukens, J. (2012). *System identification: a frequency domain approach*. John Wiley & Sons.

Pintelon, R., Schoukens, J., Vandersteen, G., & Barbé, K. (2010a). Estimation of nonparametric noise and FRF models for multivariable systems—part i: Theory. *Mechanical Systems and Signal Processing*, *24*(3), 573–595.

Pintelon, R., Schoukens, J., Vandersteen, G., & Barbé, K. (2010b). Estimation of nonparametric noise and FRF models for multivariable systems—Part II: Extensions, applications. *Mechanical Systems and Signal Processing*, *24*(3), 596–616.

Pipeleers, G., & Vandenberghe, L. (2011). Generalized kyp lemma with real data. *IEEE Transactions on Automatic Control*, *56*(12), 2942–2946.

Poolla, K., Khargonekar, P., Tikku, A., Krause, J., & Nagpal, K. (1994). A time-domain approach to model validation. *IEEE Transactions on Automatic Control*, *39*(5), 951–959.

Robel, G. (1989). On computing the infinity norm. *IEEE Transactions on Automatic Control*, *34*(8), 882–884.

Skogestad, S., & Postlethwaite, I. (2005). *Multivariable feedback control: analysis and design*. john Wiley & sons.

Smith, R. S., & Doyle, J. C. (1992). Model validation: A connection between robust control and identification.. *IEEE Transactions on Automatic Control*, *37*(7), 942–952.

Tacx, P., Habraken, R., Witvoet, G., Heertjes, M., & Oomen, T. (2024). Identification of an overactuated deformable mirror system with unmeasured outputs. *Mechatron.*, *99*, Article 103158.

Tacx, P., & Oomen, T. (2021). Accurate $\mathcal{H}_\infty$-norm estimation via finite-frequency norms of local parametric models. In *2021 American control conference* (pp. 332–337). ACC: IEEE.

Van de Wal, M., van Baars, G., Sperling, F., & Bosgra, O. (2002). Multivariable $\mathcal{H}_\infty/\mu$ feedback control design for highprecision wafer stage motion. *Control Engineering Practice*, *10*(7), 739–755.

Van Loan, C. (1978). Computing integrals involving the matrix exponential. *IEEE Transactions on Automatic Control*, *23*(3), 395–404.

Verbeke, D., & Schoukens, J. (2019). Frequency response measurements with local parametric modeling. *IEEE Transactions on Instrumentation and Measurement*, *69*(6), 3249–3261.

Vinnicombe, G. (2001). *Uncertainty and Feedback: $\mathcal{H}_\infty$ Loopshaping and the ν-Gap Metric*. World Scientific.

Voorhoeve, R., van der Maas, A., & Oomen, T. (2018). Nonparametric identification of multivariable systems: A local rational modeling approach with application to a vibration isolation benchmark. *Mechanical Systems and Signal Processing*, *105*, 129–152.

Vries, D. K., & Van Hof, P. M. D. (1994). Quantification of model uncertainty from data. *International Journal of Robust and Nonlinear Control*, *4*(2), 301–319.

Vuillemin, P., Poussot-Vassal, C., & Alazard, D. (2012). A spectral expression for the frequency-limited H2-norm. arXiv preprint arXiv:1211.1858.

Wahlberg, B., Syberg, M. B. B., & Hjalmarsson, H. (2010). Nonparametric methods for L2-gain estimation using iterative experiments. *Autom.*, *46*(8), 1376–1381.

Zhou, K., & Doyle, J. C. (1998). *vol. 104*, *Essentials of robust control*. NJ: Prentice hall Upper Saddle River.